Routing strategies for underwater gliders

Russ E. Davis [a,*], Naomi E. Leonard [b], David M. Fratantoni [c]

[a] *Scripps Institution of Oceanography, La Jolla, CA 92093-0230, USA*
[b] *Princeton University, Princeton, NJ 08544, USA*
[c] *Woods Hole Oceanographic Institution, Falmouth, MA 02543, USA*

A B S T R A C T

Gliders are autonomous underwater vehicles that achieve long operating range by moving at speeds comparable to those of, or slower than, typical ocean currents. This paper addresses routing gliders to rapidly reach a specified waypoint or to maximize the ability to map a measured field, both in the presence of significant currents. For rapid transit in a frozen velocity field, direct minimization of travel time provides a trajectory "ray" equation. A simpler routing algorithm that requires less information is also discussed. Two approaches are developed to maximize the mapping ability, as measured by objective mapping error, of arrays of vehicles. In order to produce data sets that are readily interpretable, both approaches focus sampling near predetermined "ideal tracks" by measuring mapping skill only on those tracks, which are laid out with overall mapping skill in mind. One approach directly selects each vehicle's headings to maximize instantaneous mapping skill integrated over the entire array. Because mapping skill decreases when measurements are clustered, this method automatically coordinates glider arrays to maintain spacing. A simpler method that relies on manual control for array coordination employs a first-order control loop to balance staying close to the ideal track and maintaining vehicle speed to maximize mapping skill. While the various techniques discussed help in dealing with the slow speed of gliders, nothing can keep performance from being degraded when current speeds are comparable to vehicle speed. This suggests that glider utility could be greatly enhanced by the ability to operate high speeds for short periods when currents are strong.

© 2008 Elsevier Ltd. All rights reserved.

1. Introduction

Underwater gliders are designed to have long endurance (months) and to navigate autonomously by periodically surfacing for GPS fixes and data transmission. Stommel (1989) advanced the concept and today there are at least three well-tested models (Davis et al., 2002). The operational consequence of designing for endurance is low speed (0.2–$0.4\,\mathrm{m\,s^{-1}}$), comparable to that of ocean currents and much lower than that of strong boundary currents. This severely limits the ability of glider operators to place observations where they want them and raises the question about how to route gliders through velocity fields. That is the topic of this investigation.

The terminology is made clear by considering the simplest case of a vehicle moving at speed q and heading θ (reckoned as in the complex plane, not a compass) through water that has uniform velocity **u** with magnitude u and direction ω. The vehicle's velocity over the ground is **U** with speed U and direction ϕ, here called the course over the ground (COG). These velocities are illustrated in Fig. 1. Let $u_\phi = u\cos(\omega-\phi)$ be the current component assisting motion along the track and $u_\mathrm{N} = u\sin(\omega-\phi)$ be the current component $90°$ to the left of the track. Staying on the desired path requires the cross-track component of vehicle velocity $q\sin(\theta-\phi)$ to cancel the cross-track current u_N. The heading θ and speed U made good along the desired path are then

$$\theta = -\arcsin(u_\mathrm{N}/q) + \phi, \quad U = u_\phi + q\sqrt{1 - (u_\mathrm{N}/q)^2}. \tag{1}$$

So long as $|u_\mathrm{N}| < q$ the vehicle can stay on the desired track, but the velocity made good decreases as $|u_\mathrm{N}| \to q$. A central question addressed here is about how, in more complex velocity fields, to route a glider to reach a destination as quickly as possible. For steady currents the fastest route is given by an equation with strong parallels to the ray equations for nondispersive wave propagation.

A second question addressed is about how to route gliders, operating singly or in groups in a field of significant currents, to maximize what is learned about a measured field. The reduction in error variance of objective maps is used to measure the "skill" of a particular sampling strategy. If mapping skill were to be the sole criterion, the resulting glider trajectories would be
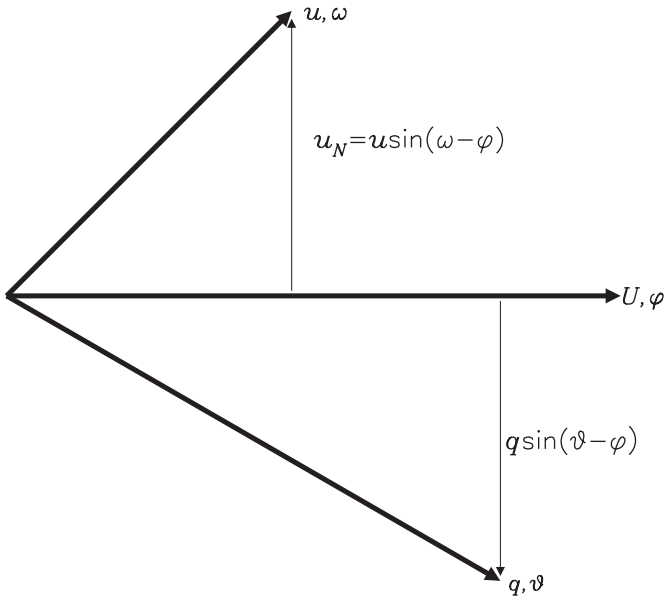
Fig. 1. Illustration of the velocities in glider steering. The vehicle's through-the-water speed and heading are q and θ, the ocean current $\mathbf{u}$ has speed and direction u and ω, and the resultant vehicle velocity over the ground is $\mathbf{U}$ with speed and course U and ϕ, respectively. Also shown are the cross-track components of through-water vehicle velocity $q\sin(\theta-\phi)$ and current velocity $u_N = u\sin(\omega-\phi)$ that cancel to give (1). The current component parallel to the track over the ground is $u_\phi = u\cos(\omega-\phi)$.

so irregular that it would be impossible to interpret them without insertion into a mapping or data assimilation procedure. Optimizing mapping skill on a network of ideal paths pre-selected to yield good observational coverage provides an automated steering procedure for optimizing both interpretability and mapping skill, including coordinating an array of vehicles.

Vehicle speed is central to both transit between points and mapping. Movement is important in mapping because mapping skill, as measured by objective analysis, increases with the number of uncorrelated observations made within a correlation time. The faster a vehicle moves, the more uncorrelated measurements it gathers. Because mapping also depends on making measurements in the right places, there is a tension between maintaining vehicle velocity to keep samples well separated and moving along a useful track in the face of currents.

2. Strategies for fast routing

Because gliders are so slow, currents have a first-order impact on vehicle speed. Here we address strategies to minimize the time required to navigate between two points through a current field. The formalism is derived in the same way Fermat's principle is used to develop ray-tracing equations for sound or light propagation (Pierce, 1989). Let the steady water velocity be $\mathbf{u}(\mathbf{x})$ while q and θ are the glider's speed through the water and its heading, respectively. The coordinates of a glider trajectory are $x(\lambda)$, $y(\lambda)$ where λ is an as yet undefined label of position along the path between endpoints $\mathbf{x}_A$ and $\mathbf{x}_B$. Finally, let $1/s$ be the speed of the vehicle along the path, equal to U in (1) above. The fastest route from $\mathbf{x}_A$ to $\mathbf{x}_B$ is the path that minimizes the travel time

$$T_T = \int_A^B d\lambda \frac{dt}{d\lambda} = \int_A^B d\lambda\, s\eta, \tag{2}$$

where $\eta = (d\ell/d\lambda) = \sqrt{(dx/d\lambda)^2 + (dy/d\lambda)^2}$ and ℓ is the arc length.

2.1. Rays for nondispersive wave propagation

In sound or light propagation, slowness s is a function of position $\mathbf{x}$ and the variation of travel time δT_T resulting from variations $\delta x(\lambda)$, $\delta y(\lambda)$ of the path is

$$\delta T_T = \int_A^B d\lambda\left\{\eta\left[\frac{\partial s}{\partial x}\delta x + \frac{\partial s}{\partial y}\delta y\right] + \frac{s}{\eta}\left[\frac{dx}{d\lambda}\frac{d\delta x}{d\lambda} + \frac{dy}{d\lambda}\frac{d\delta y}{d\lambda}\right]\right\}. \tag{3}$$

With the conditions $\delta\mathbf{x} = 0$ at $\mathbf{x}_A$ and $\mathbf{x}_B$, (3) is easily integrated by parts to

$$\delta T_T = \int_A^B d\lambda\left\{\left[\eta\frac{\partial s}{\partial x} - \frac{\partial}{\partial\lambda}\left(\frac{s}{\eta}\frac{dx}{d\lambda}\right)\right]\delta x + \left[\eta\frac{\partial s}{\partial y} - \frac{\partial}{\partial\lambda}\left(\frac{s}{\eta}\frac{dy}{d\lambda}\right)\right]\delta y\right\}. \tag{4}$$

If λ is taken as the arc length itself, then $\eta = 1$ and paths that extremize T_T obey

$$\frac{\partial}{\partial\lambda}\left(s\frac{dx}{d\lambda}\right) = \frac{\partial s}{\partial x}, \qquad \frac{\partial}{\partial\lambda}\left(s\frac{dy}{d\lambda}\right) = \frac{\partial s}{\partial y}. \tag{5}$$

When λ is the arc length, $dx/d\lambda = \cos\phi$ and $dy/d\lambda = \sin\phi$, the degenerate equation (5) becomes

$$s\frac{d\phi}{d\lambda} = \hat{\boldsymbol{\lambda}} \times \nabla s, \tag{6}$$

where $\hat{\boldsymbol{\lambda}}$ is a unit vector parallel to the path.

2.2. Ray equations for fast routes

For a vehicle moving through a current $\mathbf{u}(\mathbf{x})$, (1) shows the vehicle speed to be

$$1/s(\mathbf{x}, \phi) = \mathbf{u}(\mathbf{x}) \cdot \hat{\boldsymbol{\lambda}} + \sqrt{q^2 - |\mathbf{u}(\mathbf{x}) \times \hat{\boldsymbol{\lambda}}|^2}. \tag{7}$$

Here s depends on position, as it does in (3), and also on the direction of the path:

$$\phi = \arctan\left(\frac{dy/d\lambda}{dx/d\lambda}\right), \tag{8a}$$

which is the COG as in (1). The travel time is still given by (2) but its variation now includes, within the integral, the term $(\partial s/\partial\phi)\delta\phi$ not found in (3). This reflects the effect of COG on vehicle speed. The variation of ϕ from (8a) is

$$\delta\phi = \frac{(dx/d\lambda)^2}{(dx/d\lambda)^2 + (dy/d\lambda)^2}\left[\frac{\delta(dy/d\lambda)}{dx/d\lambda} - \frac{dy/d\lambda}{(dx/d\lambda)^2}\delta(dx/d\lambda)\right] \tag{8b}$$

and the variation of T_T is

$$\delta T_T = \int_A^B d\lambda\left\{\eta\,\nabla s \cdot \delta\mathbf{x} + \frac{s}{\eta}\left[\frac{dx}{d\lambda}\frac{d\delta x}{d\lambda} + \frac{dy}{d\lambda}\frac{d\delta y}{d\lambda}\right] + \frac{1}{\eta}\frac{\partial s}{\partial\phi}\left[\frac{dx}{d\lambda}\frac{d\delta y}{d\lambda} - \frac{dy}{d\lambda}\frac{d\delta x}{d\lambda}\right]\right\}, \tag{9a}$$

$$\frac{\partial s}{\partial\phi} = s^2\hat{\mathbf{z}} \cdot (\mathbf{u} \times \hat{\boldsymbol{\lambda}})\left[1 + \frac{\mathbf{u} \cdot \hat{\boldsymbol{\lambda}}}{\sqrt{q^2 - |\mathbf{u} \times \hat{\boldsymbol{\lambda}}|^2}}\right]. \tag{9b}$$

If, as in the wave propagation case, (9a) is integrated by parts with $\delta\mathbf{x} = 0$ at $\mathbf{x}_A$ and $\mathbf{x}_B$ to convert $d\,\delta x/d\lambda$ to δx, the result is

$$\delta T_T = \int_A^B d\lambda\left\{\delta x\left[\eta\frac{\partial s}{\partial x} - \frac{d}{d\lambda}\left(\frac{s}{\eta}\frac{dx}{d\lambda} - \frac{1}{\eta}\frac{\partial s}{\partial\phi}\frac{dy}{d\lambda}\right)\right] + \delta y\left[\eta\frac{\partial s}{\partial y} - \frac{d}{d\lambda}\left(\frac{s}{\eta}\frac{dy}{d\lambda} + \frac{1}{\eta}\frac{\partial s}{\partial\phi}\frac{dx}{d\lambda}\right)\right]\right\}. \tag{9c}$$

Now taking λ to be distance along the path (so $\eta = 1$) gives the new "ray" equations

$$\frac{d}{d\lambda}\left(s\frac{dx}{d\lambda} - \frac{\partial s}{\partial \phi}\frac{dy}{d\lambda}\right) = \left(\frac{\partial s}{\partial x}\right)_{\phi,y},$$
$$\frac{d}{d\lambda}\left(s\frac{dy}{d\lambda} + \frac{\partial s}{\partial \phi}\frac{dx}{d\lambda}\right) = \left(\frac{\partial s}{\partial y}\right)_{\phi,x}. \tag{10}$$

Comparison with (5) for sound and light propagation shows that vehicle speed takes the place of wave propagation speed and the dependence of the vehicle speed on direction, through $\partial s/\partial \phi$, adds a new term. As in (5), the two equations (10) are degenerate and can be combined to give

$$s\frac{d\phi}{d\lambda} + \frac{d}{d\lambda}\left(\frac{\partial s}{\partial \phi}\right)_{x,y} = (\lambda \times \nabla s) \cdot \hat{\mathbf{z}}, \tag{11}$$

where $\hat{\mathbf{z}}$ is a vertical unit vector. The second equation simply restates that s is a function of λ.

When wave speed depends only on y, propagation simplifies to Snell's law, $s \cos \phi = s_0$, where s_0 is a constant. This follows from (5) with $\partial s/\partial x = 0$. For glider motion, a similar relation derives from (10) when the flow is parallel, say $\mathbf{u} = \hat{\mathbf{x}}u(y)$, so that $\omega = 0$ and $\partial s/\partial x = 0$:

$$s \cos \phi - \frac{\partial s}{\partial \phi}\sin \phi = s \cos \phi - s^2 u \sin^2 \phi$$
$$\times \left[1 + \frac{u \cos \phi}{\sqrt{q^2 - u^2 \sin^2 \phi}}\right] = K/q, \tag{12a}$$

where

$$s = \frac{1}{u \cos \phi + \sqrt{q^2 - u^2 \sin^2 \phi}}. \tag{12b}$$

The transcendental equation (12) specifies the COG, $\phi(u, K)$, as a function of local speed and integration constant K, which equals $\cos \phi_0$, where ϕ_0 is the COG when $u = 0$.

Fig. 2 shows the family of solutions to the Snell's law analogue (12). Each curve is defined by a different value of $K = \cos \phi_0$. Fig. 2A shows the COG ϕ as a function of u/q for various K. Fig. 2B shows the vehicle heading θ for the same trajectories. Given K, a trajectory can be found using $\phi(u)$ from (12) and integrating $d(x+iy)/d\lambda = \exp[i\phi(u)]$. The trajectory for only a few discrete values of K would connect specified end points so that iteration on K would be required. It is conceptually and computationally simpler to directly integrate (11). The main virtue of the Snell's law analogue is that it shows how fast routing is determined both locally, by the relation between ϕ (or θ) and the local velocity, and also globally, through the dependence of K on the trajectory end points.

2.3. Examples of fast-route rays

In terms of evolution with distance λ along the trajectory, the ray equation (11) is

$$s\frac{d\phi}{d\lambda} + \frac{\partial G}{\partial x}\frac{dx}{d\lambda} + \frac{\partial G}{\partial y}\frac{dy}{d\lambda} + \frac{\partial G}{\partial \phi}\frac{d\phi}{d\lambda} = \frac{\partial s}{\partial y}\cos \phi - \frac{\partial s}{\partial x}\sin \phi, \tag{13}$$

where $G(x, y, \phi) = (\partial s/\partial \phi)_{x,y}$ is defined in (9b). To find extremal paths through the velocity $\mathbf{u}(\mathbf{x})$, the velocity field was gridded and spatial derivatives were computed by finite differences. The resultant equation for $d\phi/d\lambda$ was integrated by a fourth-order Runge–Kutta routine.

Trajectories through parallel flows are shown in Fig. 3. Position is normalized by the spatial scale of the velocity field. Trajectories start from $x = 0$, $y = 0$ and end at various x values along $y = 1$.
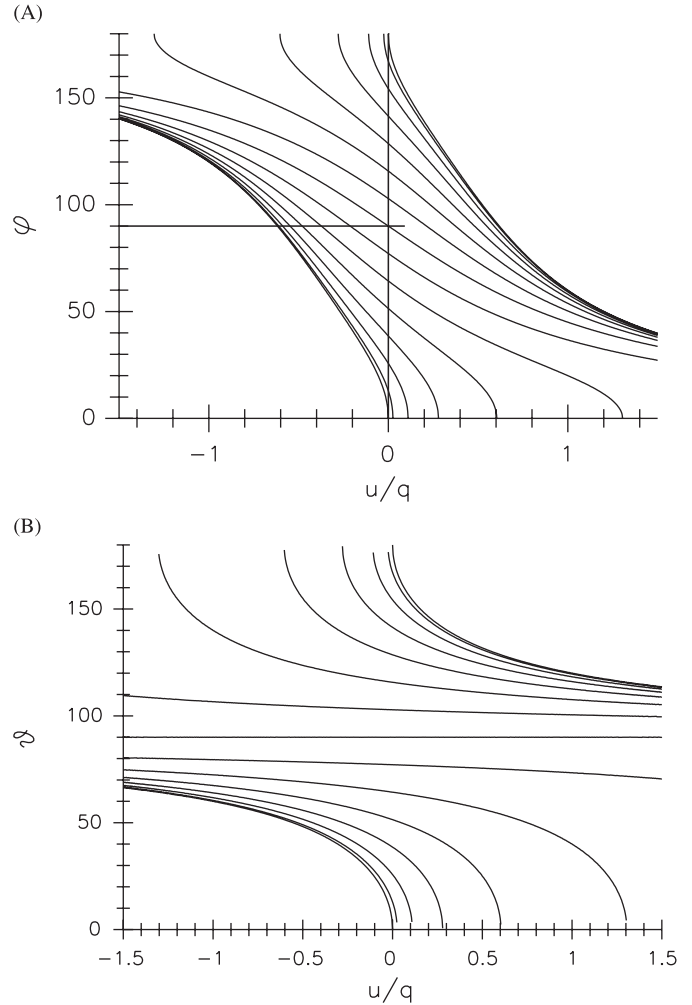

Fig. 2. (A) Solutions to (12) for parallel flow $u(y)$, where ϕ is the COG (degrees) from the x–u-axis. Only trajectories in the $+x$ direction are shown. If $\phi(u, \phi_0)$ is a solution, so is $-\phi(u, \phi_0)$. Each curve is identified by ϕ_0, the COG when $u = 0$. Solutions obey $\phi(-u, \phi_0) = \pi - \phi(u, \pi - \phi_0)$. Every point along the u/q-axis is a solution with $K = q/(u+q)$. (B) Vehicle heading θ vs. $u(y)$ for the solutions of (12) graphed in (A). Since $\phi = \theta$ when $u = 0$, one can connect solutions between the two plots. The $\theta = 90°$ curve divides solutions with a component of vehicle motion toward $+x$ ($\theta < 90°$) from solutions with headings toward $-x$. Note how, in both regions, the heading approaches $90°$ when the current becomes strong and adverse.

Fig. 3A corresponds to $u(y) = 2q \exp(-4(2y-1)^2)$ while $u(y) = (3/2)q \sin(\pi y)$ for Fig. 3B. Each trajectory is both a local and a global extremum of travel time. Also shown are the vehicle headings θ leading to the trajectory.

Finding the fastest path between two points is analogous to solving two-point boundary-condition ordinary differential equations by repetitively integrating from A using initial conditions that are adjusted until conditions at B are satisfied. The added challenge here is that there may be a family of "rays" that obey (13) and connect $\mathbf{x}_A$ and $\mathbf{x}_B$. Each is a local extremum of travel time but only one is the fastest. The multiplicity of rays connecting two points complicates the search for initial headings that reach the desired target but searching over headings, first with an exhaustive coarse-resolution search and then by repeated interpolation, has proven adequate. Fig. 4 shows the three simplest paths connecting $x = y = 0$ to $x = 0$, $y = 1$ in the parallel velocity field $u = 2q \sin(\pi y)$ where q is the vehicle speed. There are additional, substantially more complicated, longer, and more time-consuming paths connecting the same points after crossing $y = 1$ several times, which are not shown.
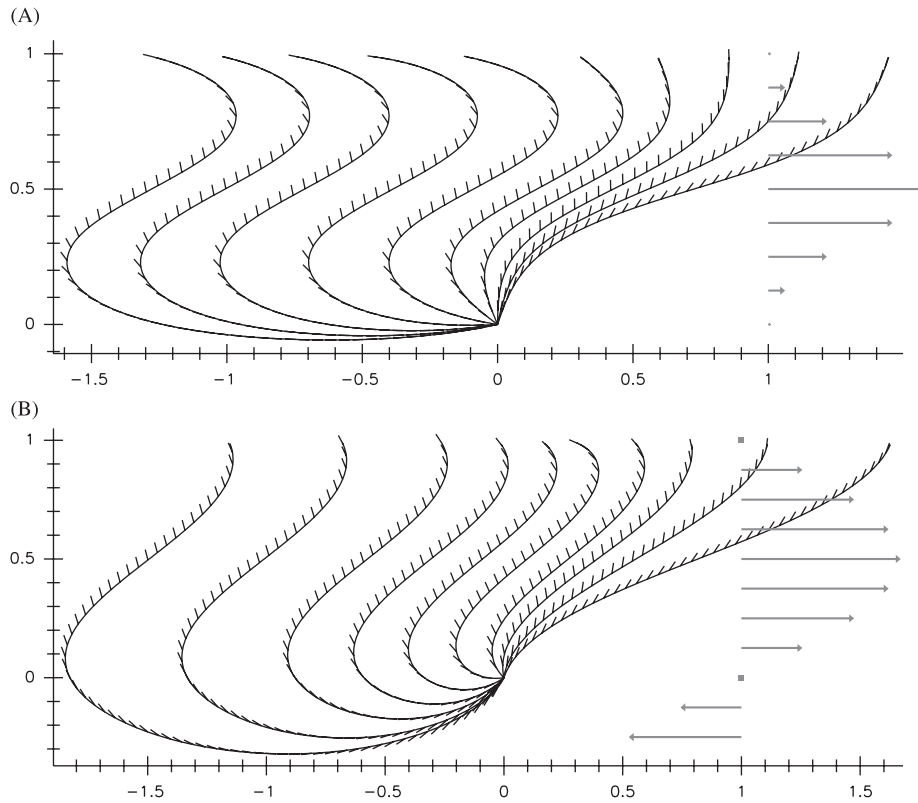
(A)

(B)

Fig. 3. (A) Trajectories from (13) for a vehicle with through-water speed q moving from $x = y = 0$ across the parallel velocity field $u(y)2q \exp(-4(y-0.5)^2)$. Velocity vectors are sketched at $x = 1$. The short tics equally spaced along each trajectory show the vehicle heading but not speed. (B) As in (A) for the parallel velocity $u(y) = (3q/2)\sin(\pi y)$.
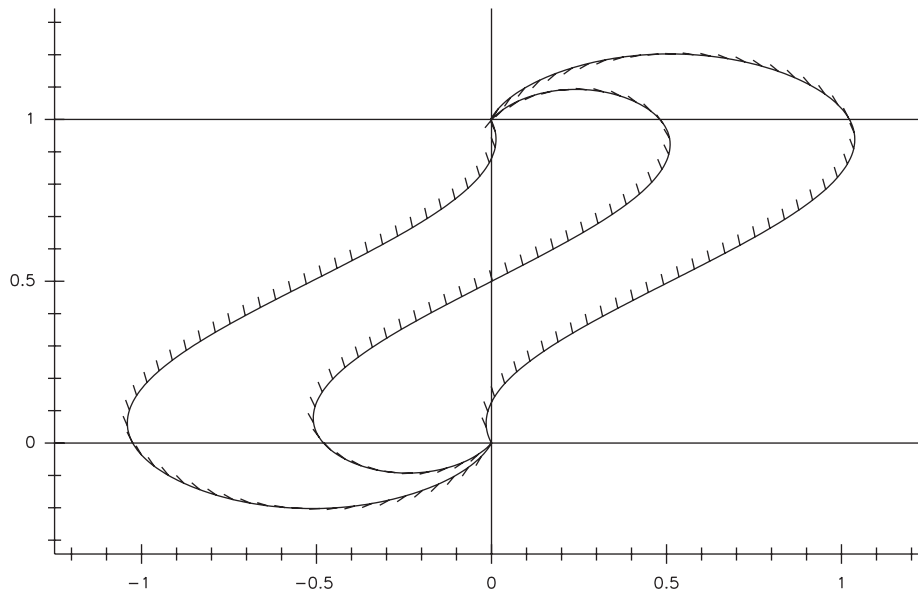

Fig. 4. Multiple travel-time extremum trajectories across the parallel flow $u = 2q \sin(\pi y)$. The central trajectory is the slowest, with a crossing time $1.97L/q$. The outer two trajectories are a symmetric pair with the crossing time $1.72L/q$. The plot format is the same as Fig. 3.

When the flow is not parallel, the strategy for rapidly reaching a destination becomes more complex. Fig. 5A shows three travel-time-extremum paths through an eddy velocity field between the same two points. The longest path is the fastest because it follows the flow, while the most direct path, which is almost directly against current, is the slowest. The same behavior is seen in Fig. 5B, which shows paths through the same circular-eddy velocity field that connect different position pairs. For the initial $x_0 < -0.5$ the fastest trajectories veer to the left to avoid the strongest adverse flow. For $-0.5 \leqslant x_0 \leqslant 0.5$ the fastest paths curve to the right to follow the flow toward the destination. And for $x_0 > 0.5$ the paths are dented toward the eddy center to pick up slightly stronger favorable currents.
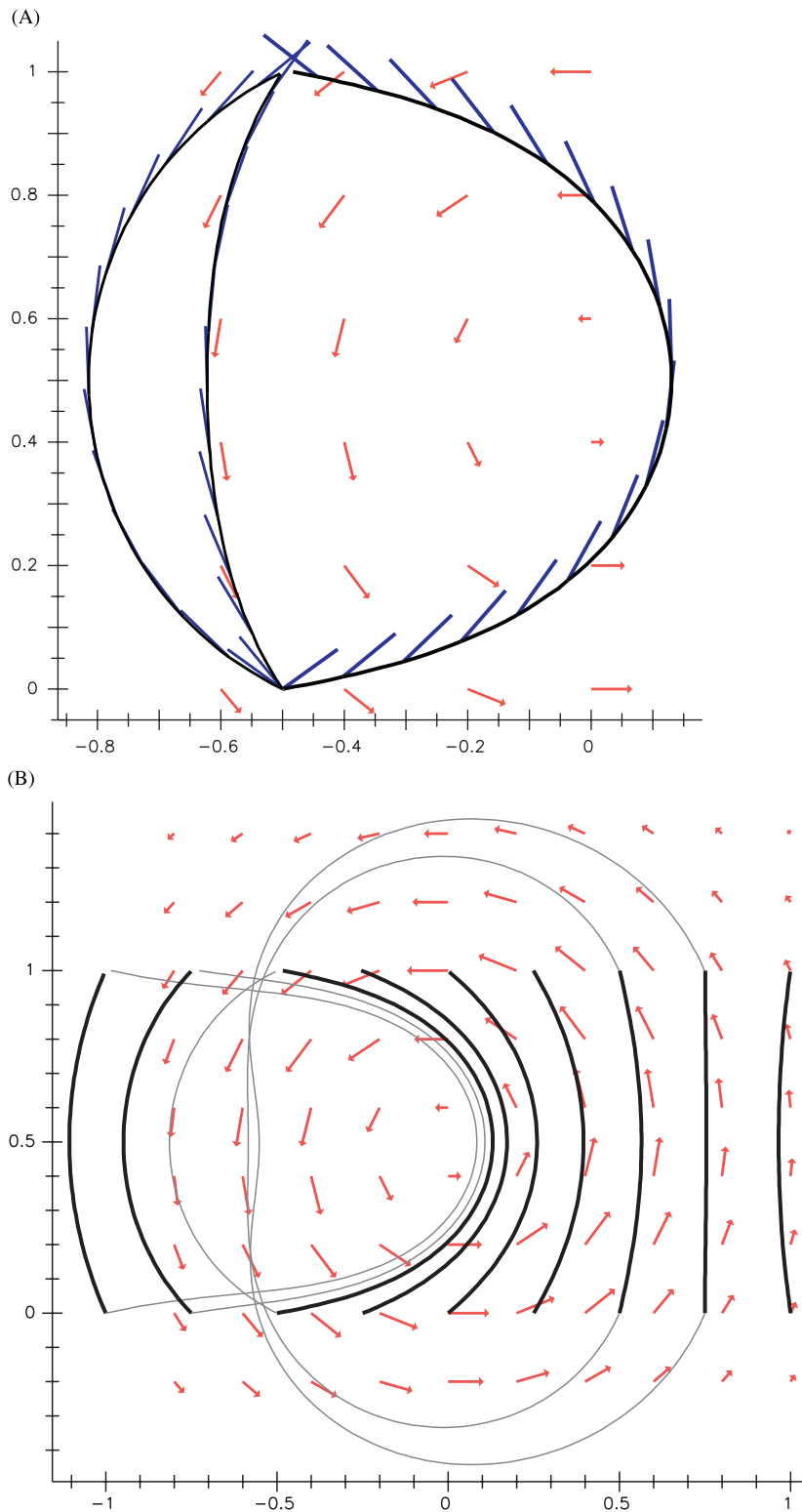
(A)

(B)

Fig. 5. (A) Paths with local travel-time extrema between $(x, y) = (-\frac{1}{2}, 0)$ and $(-\frac{1}{2}, 1)$ through a circular eddy with tangential velocity profile $qr\exp(-2r^2)$ shown with red arrows. Blue lines show the vehicle heading at positions equally spaced along the track. The long path to the right, which is aided by the flow near $y = 0$ and 1, is the fastest with travel time $1.37L/q$. The path to the left has travel time $1.29L/q$. The slowest is the intermediate path, directly opposed to the current, with travel time $2.32L/q$. (B) The fastest paths (dark black) and second fastest paths (gray) from various positions on $y = 0$ to the same x coordinate on $y = 1$ through the circular eddy in (A).

3. Local steering for fast transit

The ray equation (11) or (13) provides the fastest routes when the current field is steady and known globally. But currents are usually unsteady and (even with the best models initialized by significant bodies of data) poorly known over the time period of a typical glider transit. Consequently, a more practical but suboptimal procedure for finding good routes is needed. Two

problems must be solved: (a) a good route must be selected and updated and (b) gliders must be steered to follow these paths using noisy and infrequent velocity measurements. For steering, only a short-range velocity forecast is needed and when tidal currents are weak, even a simple persistence forecast based on the velocity between the last two fixes works well. C. Eriksen (priv. comm.) reports that using a Kalman filter to assimilate previous positions and to estimate future velocities is effective in strong tidal currents. The problem of selecting the route to be followed is far more difficult.

The structure of optimal trajectories through parallel flows suggests a way to choose good paths when the flow is neither steady nor fully known. An optimal trajectory from (13) is one member of a family of local relations between heading and current that is selected by the global requirement of reaching a particular destination. The local part provides a general steering rule for making progress through strong currents: *In a strong adverse current, steer to rapidly cross the current while making up ground where the currents are weak or favorable.* The trajectories and headings in Fig. 3 exemplify this rule. Where currents are strong, a heading with a strong cross-stream component is maintained as the vehicle is blown down current. When the current is weak or favorable, the vehicle works its way toward the destination or toward a good path to the destination. This simple qualitative rule has been used successfully when operating in strong western boundary currents and eddies.

An automated method for rapidly transiting a field of energetic currents can be developed from the above general steering rule.

Let θ_D be

$$\theta_D = -\arcsin(\tilde{u}_N/q) + \phi,$$

$$\text{where } \tilde{u}_N = \begin{cases} u_N & \text{if } |u_N| \leqslant q, \\ q \, \text{sign}(u_N) & \text{if } |u_N| > q. \end{cases} \quad (14a)$$

Here u_N is the component of the current perpendicular and to the left of the track toward the destination. This heading, based on (1), emphasizes getting to the destination following a straight line when possible. Because it does not use knowledge of future currents nor ones anywhere but the present location, the steering rule θ_D can lead to vehicles being trapped while headed into the current and making little or no forward progress. To complement θ_D, let θ_C be the direction 90° to the current that is most nearly directed toward the destination.

We have tested the steering algorithm to automatically blend θ_C and θ_D:

$$\theta = (1-w)\theta_D + w\theta_C, \quad (14b)$$

where $w = \tanh(\alpha/\sqrt{U})$, U is the component of vehicle velocity toward the destination associated with the heading θ_D as drawn in Fig. 1, and α is a scalar. The particular form for w is somewhat arbitrary and selected through experimentation to allow different α to produce a range of transitions from $w = 0$, when reasonable progress is being made toward the destination, to $w = 1$ when progress is stalled.

Performance of the steering algorithm (14) was determined by simulating pseudo-random eddy fields and steering through these fields toward a specified destination. Velocity fields were
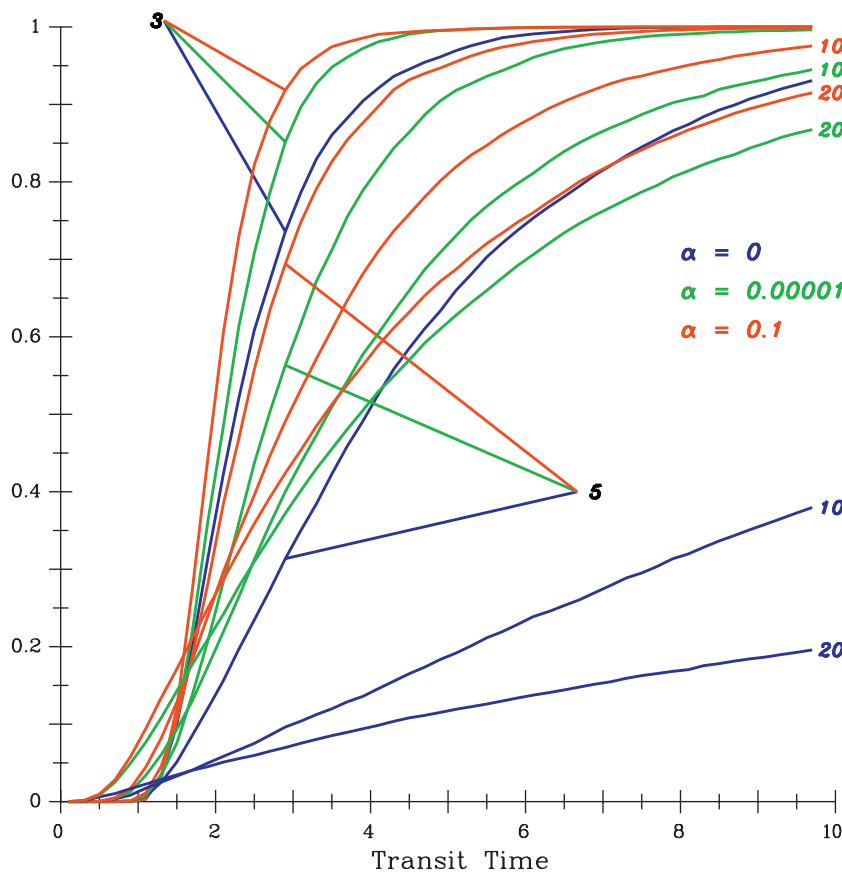

Fig. 6. Cumulative probability functions of transit time through pseudo-random velocity fields using the blended steering algorithm (14) with different values of parameter α as given by the color code in the legend. All curves are for vehicles with speed $q = 5$ going from 10 distance units to one distance unit from the destination through an ensemble of several thousand velocity fields. The rms velocity u' is given by the numerical labels. Gliders that seek a COG directly to the destination (blue curves, $\alpha = 0$) are frequently trapped by adverse currents and have long transit times. Raising α to 10^{-5} (green) substantially reduces the incidence of slow transits and increasing α to 0.1 (red) further speeds transit.

based on a streamfunction with an isotropic, homogeneous, Gaussian-shaped spatial covariance with an exponential variation in time. Velocity fields were computed from Fourier series with pseudo-random amplitudes that were drawn to have the appropriate wavenumber spectrum and evolved as first-order Markov processes. The spatial and temporal scales of the streamfunction covariance were L and T, respectively, and results are here reported in dimensionless form scaled by these scales.

Experimentation showed that the main determinants of the average speed toward a destination are the frequency and duration of periods when the vehicle was essentially trapped in a strong current while trying to follow its steering rule. The steering rule θ_D, which aims the COG directly toward the destination when possible, is particularly susceptible to trapping. The second most important determinant of transit time is behavior near the destination where strong currents can cause the vehicle to be swept past the destination, particularly if it was not steering directly toward that point. As a consequence, the performance of the generalized steering rule (14b) with various parameters α is different during transit far from the destination and during the approach phase. The choice $\alpha = 0$, which corresponds to using only θ_D, is the least prone to missing the destination whereas larger values of α accelerate transit at distances greater than one unit from the destination.

Fig. 6 shows the statistics of dimensionless transit time for vehicles going from 10 units to one unit from the destination. The approach phase has been eliminated because, as noted above, it behaves rather differently. All curves are for vehicle speed $q = 5$, which corresponds to a vehicle being able to cross O(5) eddies before the velocity field undergoes substantial time variation. This is a relatively bad situation for trapping, which is the worst when an eddy changes little in the time it takes a vehicle to cross it. Fig. 6 shows the cumulative distribution function of transit time, for various combinations of rms eddy speed u' and parameters α, computed by simulating several thousand transits. Each curve shows the fraction of vehicles making transit in a time less than the abscissa value. These curves demonstrate that when $u'/q > 1$, the steering rule θ_D is prone to trapping and long transit times. A small increase of α to 10^{-5} dramatically speeds transit under these conditions and a further increase to $\alpha = 0.1$ increases mean transit speed and reduces the fraction of very slow transits even further.

For transit outside the approach-to-destination phase, the generalized steering algorithm (14b) with a small but nonzero value for α outperforms the straight-to-the-destination steering rule θ_D under all conditions examined. When u', $q \leqslant O(1)$, the effect of α is small because trapping is less serious. But when $u'/q > O(1)$, and particularly when u'/q is also greater than unity, a nonzero α leads to heading across the current when forward progress is slow and, on average, this substantially speeds transit. Within an eddy scale of the destination, the rule θ_D corresponding to $\alpha = 0$ is safer because it minimizes the chance of being swept past the destination. Because avoiding trapping is the main goal, the shape of the tanh function used to blend θ_C and θ_D and use of $\sqrt{U}$ in its argument are not critical. The simple rule of switching from θ_D to θ_C when the U is less than some small cutoff works almost as well.

4. Routing strategies for achieving mapping skill

Gliders are, of course, intended to measure the ocean. Using a glider or two to maintain time series stations or make repeated sections does not pose any new problems in sampling. But as glider use expands to sustained collaborative sampling by fleets of gliders, it becomes increasingly important to maximize the information these fleets provide and to minimize the human

attention required to maintain effective sampling arrays. Here we examine automatic algorithms for routing gliders to maximize mapping skill in sustained arrays.

4.1. What makes a good mapping array?

Design of data-adaptive sampling arrays involves several aspects: [A] use of available data and models to define sampling objectives and performance metrics; [B] use of vehicle performance to estimate the range of achievable sampling arrays; [C] evaluation of performance metrics to determine how well achievable arrays meet the objectives; and [D] continual updating of the planned array as new information is gained. The most sophisticated implementation of data-adaptive sampling is for energy-containing scales in the atmosphere, where large lateral scales and proliferated observations make sampling dense, aircraft make it feasible to sample at planned locations and times, and skillful numerical models provide both analysis objectives and metrics for "targeting" observations. Because of these characteristics, the meteorological emphasis has been on methods of determining which additional observations will have the greatest impact on model forecasts (combining [A] and [C]). These methods include the model adjoint (Bergot and Doerenbecher, 2002), model singular vectors (Buizza and Montani, 1999), and the ensemble transform Kalman filter (Bishop et al., 2001; Majumdar et al., 2002). All these approaches are dependent on a notional linearization of the model and are successful because atmospheric observations are dense enough to make the models skillful. A focus on aircraft and satellites has made consideration of array achievability ([B]) and updating ([D]) secondary in importance.

In contrast, in oceans, scales are as short as 15 km and 2 days (Ramp et al., 2008) and subsurface observations are even more logistically difficult than atmospheric sampling. Consequently, oceans are usually too sparsely sampled to accurately initialize or verify numerical models so that analysis objectives for adaptive ocean sampling are often broader and less model oriented than in the atmosphere. For example, in the AOSN-II effort (Curtin and Bellingham, 2008), data were intended both to be assimilated by models and to directly characterize the energetic patterns and processes of variability. Sustained AOSN-II observations mainly employed repeated sampling over preplanned arrays, but the associated dialogue between modelers and observers made it clear that data-adaptive sampling was important to this kind of effort and that gliders could potentially meet that need.

Relative to meteorology, the slow speed of underwater gliders fundamentally changes the balance between the four aspects of adaptive sampling listed above. It makes achieving a planned sampling array ([B] above) as challenging as planning the array, and it makes continual updating ([D]) of both sampling targets and their achievability essential. Leonard et al. (2007) provide practical approaches for controlling gliders in the face of unpredictably changing ocean currents. Lermusiaux (2007) describes two efforts at adaptive sampling in AOSN-II that directly involve models but circumvent the problem of achieving the planned sampling array when unpredictable aspects of the ocean significantly affect the sampling vehicle and/or the places where observations will be of greatest benefit. That is the topic here.

For our focus on maintaining sampling arrays in the face of unpredictable ocean variability and currents, objective mapping (Bretherton et al., 1975) provides a good model-independent measure of sampling power. On a depth horizon, let $\mathbf{r}$ combine position $\mathbf{x}$ and time t, $w(\mathbf{r})$ be the field of interest, and $d_n = w(\mathbf{r}_n) + \varepsilon_n$ be an observation, where ε is sampling error from small-scale variability not included in w. The space–time

covariance of w is $C(\mathbf{r}_1, \mathbf{r}_2)$ and $D_{nm} = C(\mathbf{r}_n, \mathbf{r}_m) + \langle \varepsilon_n \varepsilon_m \rangle$ is the data covariance. The objective analysis estimate $\hat{w}$ of w is the linear combination of data that minimizes the mean-square error $\sum_n \langle (\hat{w} - w)^2 \rangle$ and its skill (mean-square-error reduction) is

$$S(\mathbf{r}, N) = \sum_{n,m}^{N} C(\mathbf{r}, \mathbf{r}_n) D_{nm}^{-1} C(\mathbf{r}, \mathbf{r}_m). \qquad (15)$$

Given ways to find C and D, it is straightforward to calculate the skill S for any sampling array (the collection of $\mathbf{r}_n$).

It is worth emphasizing how vehicle speed impacts mapping. From (15), the two criteria for a useful set of observations are: (a) each datum should be well correlated with w in C and (b) the correlation D_{nm} between different data should be small so they are far from redundant. If the space and time scales are L and T, respectively, over an $O(T)$ interval a time series adds little more to skill than a single observation. A vehicle sampling over a distance of $O(L)$ also gathers the equivalent of another uncorrelated observation so that over an interval of $O(T)$ a vehicle moving at the speed U gathers the equivalent of UT/L uncorrelated observations. If the operational impact of speed on vehicle endurance is neglected, speed increases the utility of a sampling platform. We do not consider slowing gliders as a way to improve mapping.

4.2. General strategies for mapping

Within the context of field studies like AOSN-II, our goal is to sustain surveillance over a specified area containing several energetic features for a period of several feature time scales. Our first approach was to search directly for the achievable array that maximizes mapping skill integrated over the time and area of interest. Trial glider trajectories were computed through specific velocity fields and the position/times of glider samples used to compute from (15) the mapping skill. A quasi-exhaustive search was used to select new tracks to increase the space–time integrated skill. Practicality motivated simplifying the candidate paths in order to reduce the number of degrees of freedom in the search. In one method, a grid was established and the gliders were made to move along rectilinear lines between the grid points. In another, vehicles were limited to a number of specific headings separated by several degrees. The results from the two simplifications applied to arrays of 5–10 vehicles were the same:

(1) Over periods comparable to the time it takes a vehicle to cross the region, "optimal" trajectories were sensible (but more complex than anticipated), well spaced, and gave mapping skills greater than would be obtained from an equal number of time series.
(2) For longer time periods the search rapidly becomes computationally exhausting. For example, if the path of a single glider consists of M segments with heading resolved to $10°$, an exhaustive search involves 36^M (over 10^{31} for $M = 20$) evaluations of mapping skill.
(3) Over long time periods the optimal trajectories were extremely complex, irregular, and spread seemingly at random across the area of interest. If the observations within one eddy time scale had been dense, this would not matter because interpolation would be accurate and the field known well everywhere. Sparse data of this type also would be useful as input for objective mapping, model assimilation, or other indirect analyses. But when the sampling is globally sparse, it would, for example, be impossible to separate time and space variability, identify time or space scales, or define characteristic energetic patterns directly from these data the

way one could from time series stations or well-sampled transects.

The third finding motivates a metric for good arrays not previously emphasized. Unless measurements are globally dense or are intended only as input for sophisticated data assimilation schemes, it is desirable that, in addition to covering the region of interest, sampling should be dense enough in time and space at some places that temporal and spatial changes are not confused so that the data can be interpreted directly. In many cases repeated straight paths will be the easiest to interpret.

Additionally, the third finding has important consequences for the definition of good arrays in terms of achievability. Optimal solutions for the space–time mapping skill necessarily determine position–time trajectories for all gliders. Along complex irregular trajectories, the optimal relative glider positions will vary in a complex way. In the presence of currents, gliders will not be able to track trajectories perfectly. Even if they are steered close to the desired path, they will not also be able to match the prescribed timing of their motion along the path. In fact, if the gliders are well distributed, some may be aided by the currents and some hindered by the currents. Feedback can be used to try to correct for errors in relative positions, but this will become an intractable problem in the case of complex, irregular trajectories. As a result, in field sampling, performance may deviate significantly from the optimal.

Because achieving high temporal and spatial density of observations requires concentrating globally sparse observations on relatively simple repeated paths, and because simple paths allow systematic approaches to coordinated tracking control, we have investigated a general approach to coordinated adaptive glider sampling arrays that involves three steps:

(1) Using objective mapping as a guide for density and coverage, a relatively dense network of sampling paths covering the area of interest is defined.
(2) Based on new sampling objectives, "ideal paths" are periodically selected from the network of paths to (a) provide necessary mapping skill under predicted or climatological currents and (b) be simple enough that the results can be analyzed directly.
(3) By suitable control, multiple gliders are steered to stay near the ideal paths while maintaining spacing and speed so that sampling skill is maintained. Staying on the ideal path may be impossible if the current is strong and may degrade mapping skill if it reduces vehicle speed significantly.

Leonard et al. (2007) describe a similar approach where in step (2) the ideal paths also define the ideal relative positions along those paths that maximize mapping skill and step (3) is addressed with a control algorithm that keeps gliders close to ideal paths while maintaining the prescribed inter-vehicle spacing. Here we examine instead control of vehicles using direct feedback of mapping quality.

A suitable metric for mapping quality over the collection of ideal paths $\mathbf{x} = \mathbf{p}(\lambda)$ at time t is the path-integrated skill

$$\begin{aligned} \Sigma(t, N) &= \int d\lambda \, S[\mathbf{p}(\lambda), t, N] \\ &= \sum_{n,m}^{N} D_{nm}^{-1} \int d\lambda \, C[\mathbf{p}(\lambda), t, x_n, t_n] C[\mathbf{p}(\lambda), t, x_m, t_m], \end{aligned} \qquad (16)$$

where there are N observations and the integral extends over all the ideal paths. Maximizing Σ involves a balance between keeping vehicles close to the ideal path where skill is measured, keeping them well spaced, and maintaining vehicle speed. For a single
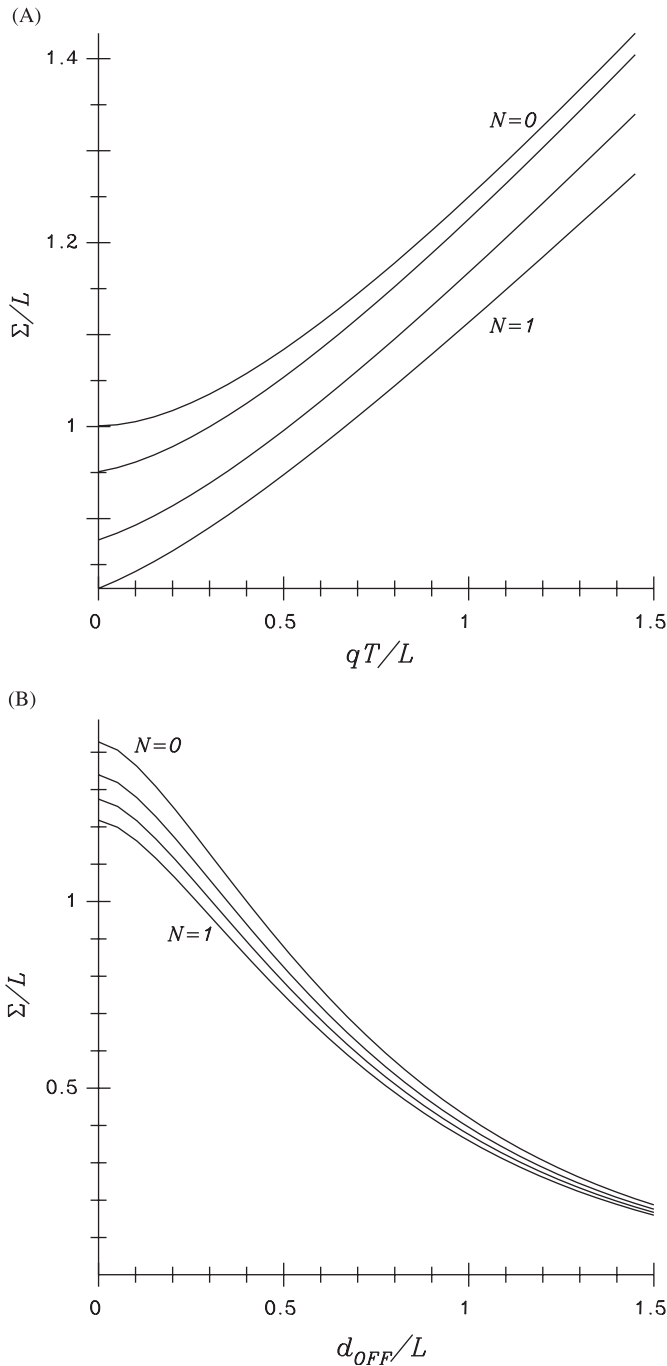
(A)

(B)

Fig. 7. (A) Integrated mapping skill Σ for a long, straight ideal path and a vehicle moving at speed q along that path. The field's covariance is exponential with length and time scales L and T, respectively, and samples are taken every $\tau = T/15$. Curves from top to bottom correspond to noise-to-signal ratio $N = 0$, 0.2, 0.5, and 1.0. Skill increases with speed and decreases with N. (B) Integrated skill Σ on a long straight path for a vehicle moving at speed $q = L/T$ on a straight sampling path displaced by d_{OFF} from the parallel scoring (ideal) path. L and T are the scales of the mapped field's exponential space and time covariance, respectively. Curves from top to bottom correspond to $N = 0$, 0.5, 1.0, and 1.5. Skill decreases as N increases.

vehicle moving along a long straight ideal path far from its ends, mapping skill is focused near and somewhat behind the vehicle's instantaneous position and decays away from that point. Fig. 7 describes the effect of vehicle speed, noise, and off-path distance on the integrated skill along a single straight ideal path when the signal covariance is $C(\mathbf{x}_1,t_1,\mathbf{x}_2,t_2) = \langle a'^2\rangle \exp(-|\mathbf{x}_1-\mathbf{x}_2|/L-|t_1-t_2|/T)$. Measurement noise variance is $N\langle a'^2\rangle$, and

measurements are made at time interval $\tau = T/15$. Fig. 7A shows how rapidly skill increases with vehicle speed q and decreases with noise ratio N. Increased speed provides more uncorrelated data. For comparison, Fig. 7B shows the integrated skill for straight vehicle tracks that are displaced from the ideal path, where skill is computed. Not surprisingly, skill decays on the scale L. While a straight ideal path is oversimplified, Fig. 7 does describe the characteristic scales involved in the balance between maintaining a vehicle's speed and keeping it near the desired track.

4.3. Steering by instantaneous mapping skill

To maximize the time integral of Σ over the period of interest by adjusting complete vehicle trajectories over this period would be a demanding computation needing to be repeated whenever new information comes in. Here we explore a much simpler approach for routing a collection of M gliders, each following its own ideal track and asynchronously producing measurements on the interval τ. The principle is simple: each time a vehicle is ready for new instructions it is steered toward the position where its next measurement will add the most to the path-integrated skill Σ of (16), without regard to future observations made by other vehicles.

Specifically, when glider A surfaces at position, time $\mathbf{x}_N$, t, the array has made N observations and the integrated skill is $\Sigma(t,N)$. Let $\hat{\Sigma}(t + \tau, N + 1)$ be the skill at time $t+\tau$ obtained from those N data plus that from glider A at its next position $\mathbf{x}_{N+1}$. $\nabla\hat{\Sigma}$, the gradient of hypothetical skill $\hat{\Sigma}(t + \tau, N + 1)$ with respect to the glider's next position $\mathbf{x}_{N+1}$, is computed by finite differences of $\hat{\Sigma}$ between positions around a likely $\mathbf{x}_{N+1}$. This gradient and the distance that the glider can make good over time τ along various courses define the heading that maximizes the future skill $\hat{\Sigma}(t + \tau, N + 1)$. In the absence of currents, $\nabla\hat{\Sigma}$ directs a single vehicle toward its ideal track but the distance made good over interval τ in the face of currents and the spacing from other vehicles can drive it off the ideal path to maintain speed and/or spacing.

Behavior of this basic procedure is easily adjusted by transparent modifications. One modification can be desirable when the ideal track has segments that intersect at angles more acute than about 120°. Experimentation shows that trajectories from the unmodified procedure often reverse direction near such intersections. The reason is simple. On a straight path, a vehicle is driven to continue its motion down the ideal path because this increases skill by making the next measurement poorly correlated with previous observations. A sharp turn in the ideal path decreases the rate at which motion down the path decorrelates new data from old, $\nabla\hat{\Sigma}$ becomes weak, and a reversed course may result. This doubling back does not decrease instantaneous path-integrated skill, but if it leads to vehicles approaching each other this can be deleterious to future skill or to interpretability. Skill will be lost when oppositely directed vehicles later come close and their measurements become partially redundant. When vehicles on a path are reflecting off each other in the presence of currents, their motion quickly becomes chaotic and this could affect interpretability. In other circumstances, particularly when the path of interest is not closed, doubling back may be a desirable feature.

The tendency for vehicles to turn back at vertices can be reduced by adding a "drift bias" vector $\mathbf{b}$ pointing toward the next intersection to the gradient $\nabla\hat{\Sigma}$ that determines how the vehicle will move. When this drift bias is adjusted to be much less than a typical skill gradient but large enough to overcome weak reverse gradients near the track vertices, vehicles tend to keep moving forward. This correction can be used to avoid future loss of skill or
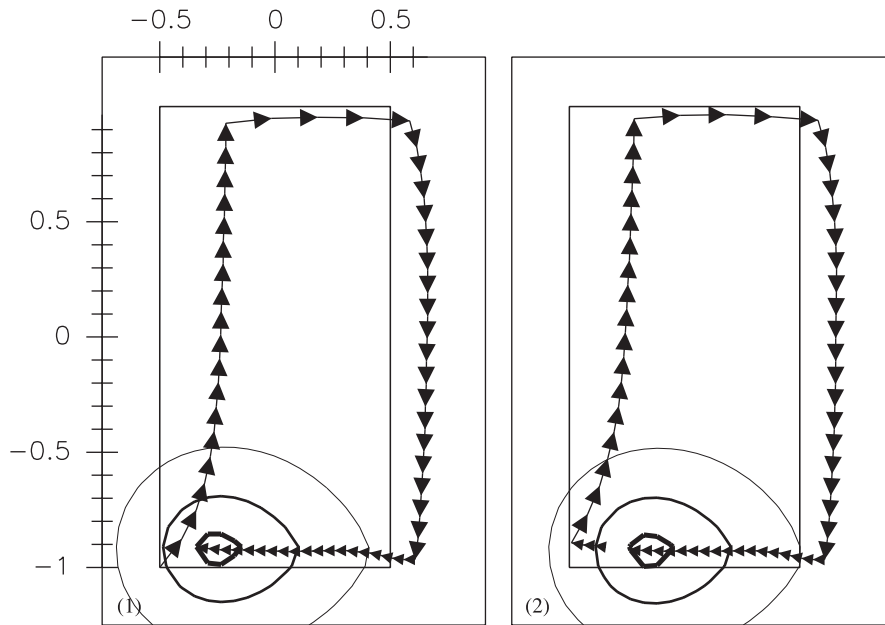
Fig. 8. Path and mapping skill of a vehicle steering to maximize ideal-path skill $\hat{\Sigma}$ on the rectangular path shown. All variables are normalized by the space and time scales L and T, respectively, of the mapped field's exponential covariance. Vehicle speed is $q = 2.5$ and a current with $u = 1.5$ flows from left to right. Each arrowhead tip marks the position of a sample taken at fixed intervals of $\tau = 0.05$ with noise/signal ratio $N = 0.2$. Light, medium, and dark oval contours are the 0.4, 0.6, and 0.8 skill contours at the time of the last position in each panel. Panel (2) follows (1) immediately. Note how the vehicles are diverted down current at the start of each cross-stream, giving up closeness to the ideal path to maintain speed and thus optimize mapping ability.
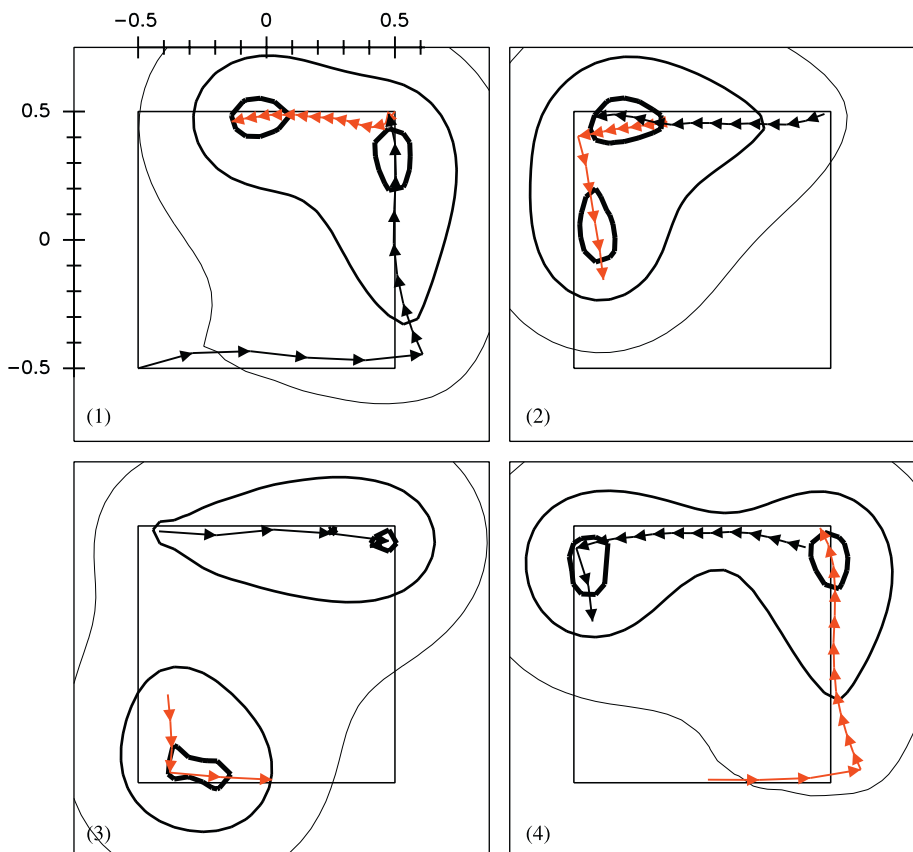

Fig. 9. Illustration of how the skill-gradient procedure maintains vehicle separation. Two vehicles (black and red) are on the square ideal track shown and their drift biases encourage counterclockwise motion. Red has speed $q = 2.5$ while black's $q = 3$ causes it to overtake red. The current, mapping-skill contours for the combined array, and other parameters are as in Fig. 8. Sequentially numbered panels follow each other immediately. In (1), red is slowed by the current, which bunching. In (2), separation changes little as black approaches the upper-left corner. In (3), black reverses course at the corner to avoid bunching that would degrade mapping skill. In (4), black returns to its initial direction of motion now well separated from red.

to increase the ability to directly analyze the data, but only at some loss of instantaneous skill.

Experimentation shows that the tracks that maximize $\hat{\Sigma}$ differ from tracks of vehicles controlled to stay near the ideal track mainly when the cross-track current is substantial. Vehicles controlled to stay on the ideal track tend to point into the current to stay on the path and consequently slow down. By trading off-track position for speed, skill can be increased. Fig. 8 shows the track from a vehicle on a rectangular ideal track in the face of a current with speed $u_x = 0.6q$. On each cross-stream leg the vehicle diverts off the ideal-path down current to maintain speed and mapping skill at the expense of cross-track distance. If current-induced departures from the ideal path are judged as too large, skill can be sacrificed to keep the trajectory closer to the ideal track by directing gliders along $\nabla(\hat{\Sigma} - \gamma \ell_x^2) + \mathbf{b}$, where γ is a positive adjustable weight, ℓ_x is the cross-track displacement, and $\mathbf{b}$ the drift bias. Increasing γ draws the vehicle toward the ideal track.

The skill-gradient procedure coordinates multiple vehicles to maintain spacing because when two vehicles approach each other, skill decreases as observations become redundant. Eventually, one vehicle will move off the track or reverse course in order to increase separation and, thereby, increase mapping skill. This is shown in Fig. 9, where two vehicles with differing speeds circulate around a path and bunch up when one overtakes the other. The trailing vehicle reverses course twice in order to preserve spacing before continuing pursuit.

Fig. 10 shows how the local skill-gradient procedure coordinates four gliders assigned to adjacent rectangular ideal tracks. The drift biases encourage opposite rotation on the two adjacent paths and the symmetric initial positions $x = \pm 0.5$, $y = \pm 1$ encourage near collisions as vehicles approach each other on the common path segment. The figure shows how the skill-gradient procedure leads to course reversals that avoid or rapidly repair near collisions and lead to coordination that maintains separation along both ideal paths.

Virtues of the local-skill-gradient method of coordinating an array are that it does not require a long-range forecast of currents, it is conceptually simple and easy to implement, and it coordinates multiple vehicles on arrays of arbitrary shape. Changing the array configuration in order to adapt to new information or goals requires only defining new ideal tracks and perhaps choosing new bias vectors. The most accurate map is obtained with zero bias and zero off-track penalty, but these parameters can be used to simplify behavior and consequently make the data easier to interpret. It is necessary only to forecast the advecting currents over the next time step the way any steering algorithm would. The procedure coordinates arrays of multiple vehicles to avoid vehicle bunching and balances the increases in mapping skill coming from proximity to the ideal track and good vehicle speed. Because the skill gradient establishes coordination, the inter-vehicle spacing is irregular when separations are much greater than the correlation scale of mapped
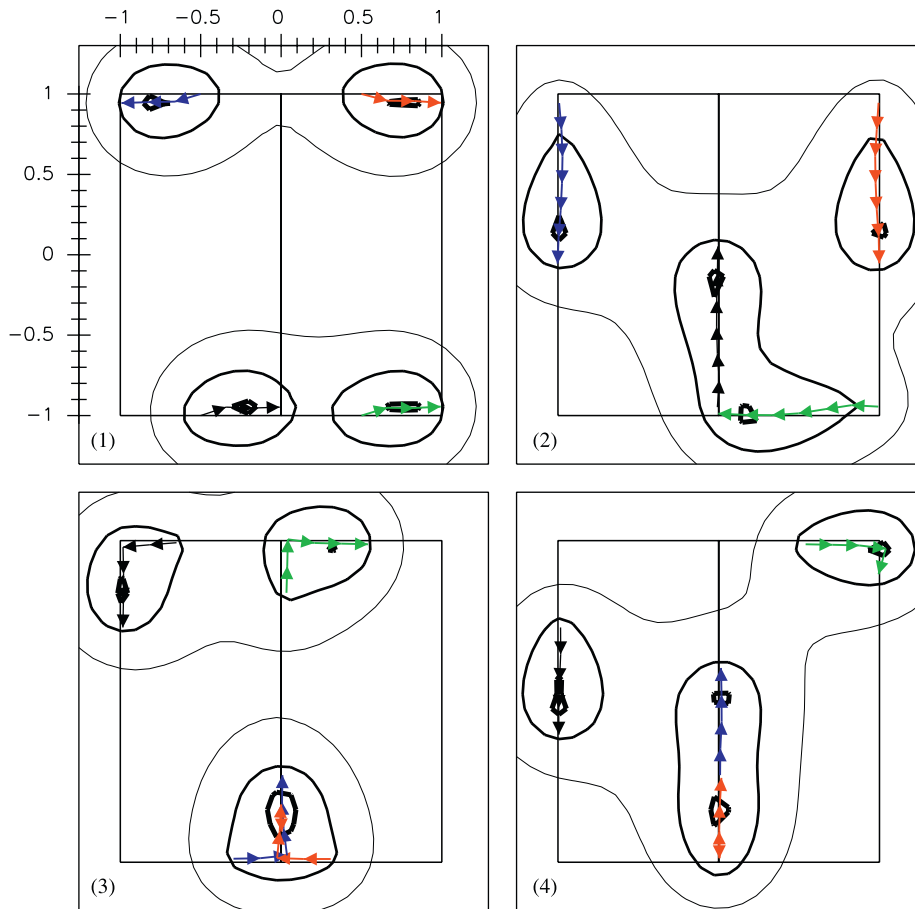

Fig. 10. Illustration of array coordination by the skill-gradient procedure. Four vehicles begin at $x = \pm 0.5$, $y = \pm 1$. Their drift biases tend to keep black and blue on the left rectangle in counterclockwise motion while clockwise motion of red and green is encouraged on the right rectangle. Vehicles move with $q = 2.5$. Everything else is as in Figs. 8 and 9. In panel (1), proximity to black causes green to reverses its normal direction to maintain spacing. In (2), red and blue continue symmetrically while green returns to its preferred sense of rotation, now following black. In (3), black and green continue their default motion while red and blue nearly collide, after which red reverses motion to gain separation. In (4), red reverses direction again to follow blue at an acceptable separation so that all vehicles follow their default motion without excessive bunching.

field. While the gaps that develop this way do not affect the track-integral estimation skill Σ, a control procedure such as that described by Leonard et al. (2007), which is based on physical separation, rather than directly on mapping skill, is more effective in enforcing uniform spacing of widely separated vehicles.

The intrinsic weakness of the skill-gradient procedure is reliance on instantaneous skill. Like any local optimization, it can miss "global" optima that maximize the time integral of skill while maximizing "local" instantaneous skill at each time. Further, because skill varies on the correlation scale, the procedure becomes ineffective if strong currents push vehicles far from their ideal tracks.

There are also practical limitations. Evaluating the skill integral $\hat{\Sigma}$ and its gradients can be slow, but, because computing the gradient of $\hat{\Sigma}$ involves arrays that differ at only one point, the technique in Appendix A dramatically speeds up calculations. Communication can be a problem if currents cannot be accurately predicted over two dives. The $\nabla\hat{\Sigma}$ that determines the desired COG and the steering to achieve that track both depend on predicting currents over the next dive, and ideally this prediction would be based on the latest position information. This requires a glider to wait on the surface after reporting its position until its optimal heading is computed at a central location where all glider positions are known. The surface is both dangerous and where currents are strongest, so extending the surface interval for calculation and communication delays is undesirable. If currents can be well predicted over two dives, the delay can be minimized by computing the steering instruction before a glider surfaces. But in cases like AOSN-II, where internal tides and fronts decorrelate velocity in a fraction of a day, there can be a big penalty for basing predictions on currents measured not over the last dive but over the one before that. However, AOSN-II gliders were coordinated to maintain triangular formations using automated steering computed with current predictions two dives old (Fiorelli et al., 2006). Likewise, in the Adaptive Sampling and Prediction (ASAP) 2006 Monterey Bay field experiment, gliders were coordinated onto ideal sampling tracks using the automated control algorithm of Leonard et al. (2007) also with current predictions two dives old.

The $\nabla\hat{\Sigma}$ procedure has not been field tested and we have only simulations like those in Figs. 8–10 to motivate further investigation of the utility, robustness, and tuning of array coordination procedures based directly on mapping performance. A desirable extension would incorporate imperfect but still useful forecasts of currents into the steering rule. Of course, the extension to performance metrics other than the ideal-path mapping skill Σ is straightforward.

5. Local steering for mapping

The trajectory ray equation of Section 2 for fast routing requires accurate knowledge of the global current field while the skill-gradient procedure for mapping in Section 4 requires knowing the positions of all gliders in the array. Both methods are automatic in the sense that the operator makes no steering decisions and only alters the control algorithm's parameters. However, both procedures depend on communicating substantial information to gliders. Just as the "local" steering procedure for rapid transit in Section 3 eliminates the need for global current information, a simpler steering procedure for mapping that requires less knowledge and communication and allows more operator intuition may sometimes be useful. Commonly, gliders select the heading that gives a track toward the next waypoint if the estimated current is correct. The appropriate heading is re-evaluated after each new position and current estimate are obtained. Here we examine an elaboration of this procedure that maintains mapping skill along ideal paths. In this mode, a glider uses its own ocean-velocity estimate and navigation to steer close to its ideal path while the operator controls the steering-algorithm parameters. Coordination of multiple vehicles can be achieved only by operator adjustments like moving waypoints to maintain vehicle spacing.

In this method of maintaining mapping skill, an off-track glider steers back toward its ideal track, but slowly enough that speed and, hence, mapping ability are not seriously impeded. Let $\mathbf{x}_C$ be the point on the ideal path closest to the vehicle and $\mathbf{x}_S$ be the position farther down the path by the distance Λ. An off-track glider takes the heading that would, if estimated currents were accurate, give a track toward the "steering point" $\mathbf{x}_S$. Whenever a glider gets another fix and velocity estimate, its position along the track, $\mathbf{x}_C$, is recomputed and advanced by Λ to find a new steering point $\mathbf{x}_S$ and the vehicle takes the heading θ toward $\mathbf{x}_S$ given by (1).

A desirable elaboration of this procedure helps keep strong cross-track currents from bringing the vehicle to a stop while heading into the flow to get back on track, much the way speed is preserved in (14). This is done by limiting the difference between heading θ and desired COG ϕ according to

$$|\theta - \phi| \leqslant \beta, \tag{17}$$

where β is an adjustable constant.

Typical mapping performance of local steering depends on the scales of the mapped field and eddy velocity, on the rms advecting velocity, vehicle speed, and the parameters Λ and β. The trade-offs involved in selecting the parameters are here described using the ideal-path-integrated mapping skill Σ of (16) on a long, straight ideal track. The path-average skill $\langle\Sigma\rangle$ was averaged over many simulations in which vehicles steered through pseudo-random velocity fields using steering points. Skill was based on isotropic, homogeneous mapped-field and eddy-streamfunction covariances that were Gaussian in space lag and exponential in time separation with both fields having the same space and time scales L and T. Velocity was computed from a streamfunction expressed as a Fourier series with appropriate wavenumber spectra and pseudo-random normally distributed amplitudes that evolved as first-order Markov processes, giving the covariance exponential temporal variation.

The parameters governing $\langle\Sigma\rangle$ are vehicle speed q and the rms speed u' of the random velocity field. Both are here nondimensionalized by the eddy time and space scales. Fig. 11 shows how, for fixed Λ and β, as the eddy velocity u' increases the rms off-track distance y' increases and the average vehicle velocity toward the destination decreases. Both of these trends reduce $\langle\Sigma\rangle$ as u' increases. The integrated skill begins declining significantly as u' exceeds $0.5q$ and is approximately halved when u' reaches q.

The optimal steering length Λ and off-course limit β depend on vehicle speed q and rms eddy velocity u'. Dependence of performance on the steering distance Λ is relatively simple. As Λ increases, so does the typical off-track distance (because the vehicle is less strongly controlled onto the track) but net velocity to the destination increases (as the vehicle spends less of its velocity getting back on track). Fig. 12 shows how mapping skill, which is oppositely influenced by these tendencies, varies with Λ for a collection of vehicle speeds and rms eddy velocities. When $u' \geqslant q$, integrated skill depends primarily on the ratio u'/q, not the speeds themselves, and strong control by $\Lambda \leqslant 1$ gives the best performance. When $u' < q$, the steering distance has little effect on skill although $\Lambda \leqslant 1$ is still the best, and performance depends on both u' and q individually, not just through u'/q.

The parameter β of (17) keeps vehicles from heading into cross-track flows and using all their forward velocity trying to get
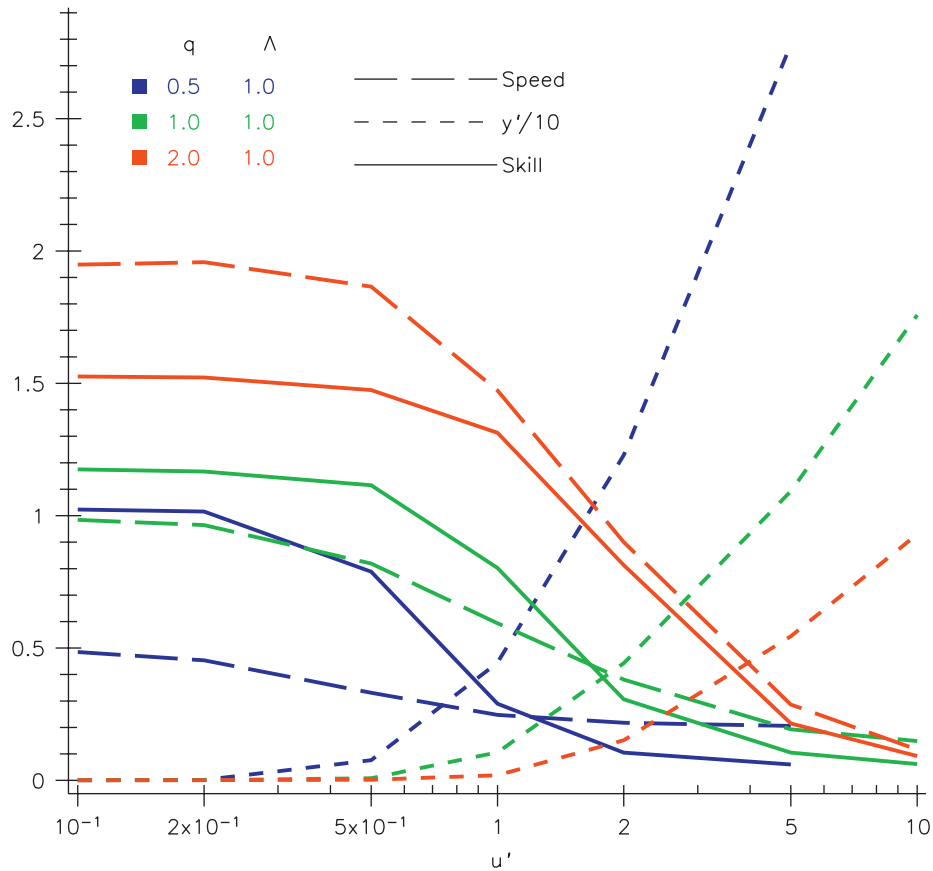
Fig. 11. Average along-track velocity (long dash), off-track distance y' (divided by 10, short dashes), and integrated mapping skill $\langle \Sigma \rangle$ (solid) for local steering on a long, straight ideal path as a function of rms eddy velocity u' for three vehicle speeds, q, as color coded in the legend. The steering distance is $\Lambda = 1$ and the off-course limit is $\beta = 60°$. Note how rms off-track distance y' increases with u' while net velocity and integrated skill decrease. Skill is halved from its no-eddy value near $u' = q$.
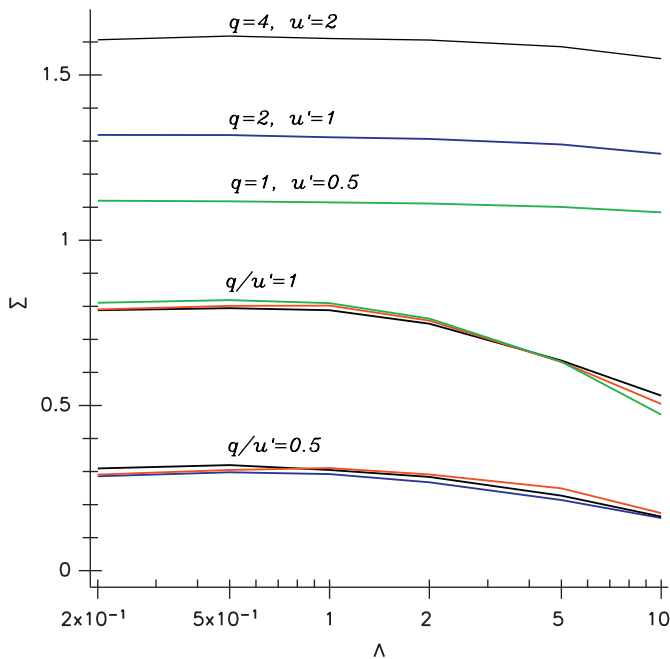

Fig. 12. Average integrated skill $\langle \Sigma \rangle$ as a function of steering distance Λ from various combinations of vehicle speed and rms eddy velocity. The curves labeled $q/u' = 0.5$ are for (u', q) pairs $(1, 0.5)$, $(2, 1)$, and $(4, 2)$. The curves labeled $q/u' = 1$ are for pairs $(0.5, 0.5)$, $(1, 1)$, and $(2, 2)$. When $u' > q$, off-track displacements are significant, skill is significantly decreased, and $\Lambda \leqslant 1$ reduces the degradation. When $q > u'$ there is a small benefit to keeping $\Lambda \leqslant 1$.
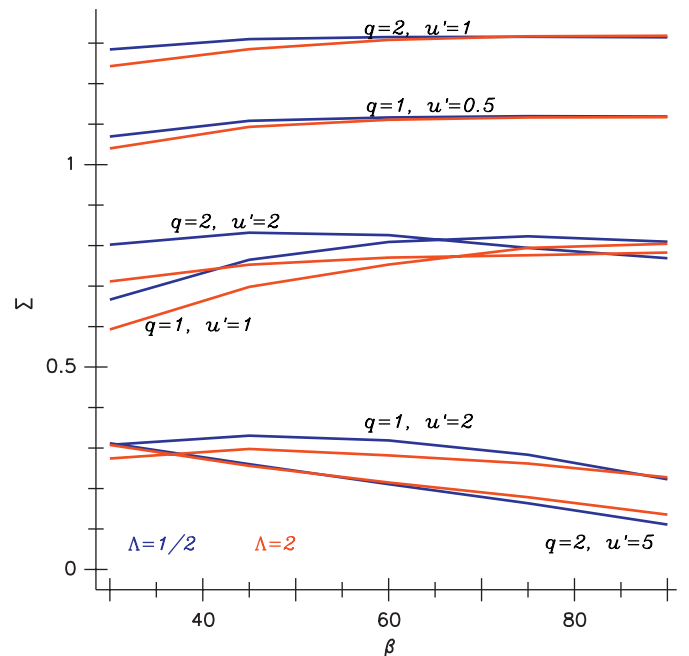

Fig. 13. Dependence of the average integrated mapping skill $\langle \Sigma \rangle$ on the off-course limit β. For each u', q combination, curves are shown for $\Lambda = 0.5$ and $\Lambda = 2$. For $u' > q$, limiting the heading to significantly less than 90° from the ideal track improves performance. But for $u' \leqslant q$, limiting the off-course heading is deleterious.

close to the ideal path. Dependence of performance on β is shown in Fig. 13. For $u' > q$ the behavior is as expected; β significantly affects skill and $\beta < 60°$ improves performance because maintaining speed is dominant. When $u' \leqslant q$, the loss of control required to stay near the ideal track caused by small β is more important than the improvement in forward speed and $\beta \approx 90°$ is optimal.

6. Conclusion

We have addressed the challenge that the slow operating speed poses to gliders accomplishing two tasks: (a) transit from point to point as required for operations and (b) sampling a region over an extended period. Current velocities are often comparable to vehicle velocities and make both tasks difficult. The problem of routing for rapid transit through a known frozen velocity field admits the simple solution discussed in Section 2. This procedure, which is similar to ray tracing for nondispersive waves, provides a way to compute optimal transit routes under these restrictions. It also provides a simple steering rule: *in a strong adverse current, steer to rapidly cross the current while making up ground where the currents are weak or favorable.*

Because current fields are usually unsteady and imperfectly known, a rapid-transit procedure is needed that accounts for time variability and limited knowledge of the velocity field. We tested such a procedure, based on the simple steering rule, in which the vehicle heads directly to the destination when good progress is possible and heads across the current when progress is slow. This procedure is particularly valuable when the velocity field evolves slowly (when a vehicle can cross a typical eddy in a time short compared to the temporal eddy scale). In this case, vehicles trying to head directly to the destination are easily trapped by strong adverse currents until time variability leads to their release. A simple steering algorithm that directs vehicles across the current when forward progress is slow dramatically reduces trapping and decreases typical transit times.

Routing gliders to maximize sampling power is more complicated. First, a performance metric is needed. Rather than one of the sophisticated model-based criteria used to target observations in meteorology, we used objective mapping error to score mapping accuracy, although this fails to account for the added information that can be extracted from dynamical laws by data-assimilating models. Second, there is an intrinsic tension between maximizing the accuracy metric and retaining an observational array that allows direct analysis of the data without a complex analysis method like objective mapping or data-assimilating models. When observations are too sparse to support accurate mapping everywhere, directly maximizing global mapping accuracy leads to arrays that are irregular and lack the dense sampling required to, for example, separate spatial variability from temporal. This tension led to an approach that begins from a set of "ideal tracks" whose occupation at a normal operating speed provides good sampling coverage and, at the same time, provides data that can be interpreted directly. In real time, a subset of these tracks is selected to meet an adaptive sampling requirement and vehicles are operated, in the face of currents, on this subset of tracks.

Scoring performance with the mapping skill integrated over all ideal paths encourages vehicles to stay close to these paths while maintaining speed and spacing, all of which increase mapping skill on the ideal tracks. Two approaches were taken to maintaining path-integrated skill. In the more elaborate approach, when a glider surfaces it is steered in the direction that adds the most to instantaneous network-integrated skill. This requires good communication and speedy steering-instruction calculation, but automatically coordinates a fleet to avoid the bunching that

degrades mapping while keeping the vehicles close to the ideal path and moving forward. This procedure, which is based on improving instantaneous skill, is vastly simpler but theoretically performs worse than a procedure that optimizes the sampling path over the full time period of interest, although achievability of this optimal sampling path is questionable because of the complexity of trajectories and the limited accuracy of current forecasts needed to direct gliders in strong currents.

We also tested a simpler procedure of controlling vehicles for sampling that uses a simple first-order control loop based on a "steering distance" Λ over which each vehicle tries to get back on its ideal track. By adjusting Λ an operator can alter the balance between off-track distance and forward speed and maximize mapping skill or favor the characteristic that is most important in a particular circumstance. The results of simulating sampling pseudo-random eddy fields suggest choosing Λ to be equal to, or less than, an eddy length scale.

While the various techniques discussed help in dealing with the slow speed of gliders, no routing procedure can keep performance from being significantly degraded when the magnitude of perturbing currents becomes comparable to the vehicle speed. This suggests that the optimal long-duration autonomous underwater vehicle (AUV) should operate at slow speeds to optimize endurance but should be able to operate temporarily at significantly higher speeds when currents are strong.

Perhaps most conspicuously missing from the methods discussed here is a way of making good use of incomplete and inaccurate but still useful information about currents. Just like advancing gliders in a model simulation, the rapid-transit ray-tracing procedure requires perfect knowledge of the current field while all the other procedures depend only on the instantaneous currents at the locations of vehicles. What is needed is a way of retaining some of the flexibility and noise tolerance of the local-steering procedures while making use of whatever global information on currents is available. It is challenging to effectively use inaccurate current predictions because glider trajectories are so sensitively and nonlinearly dependent on small errors (indeed the trajectory equations are unstable almost everywhere).

Appendix A. Efficient calculation of mapping skill increment

The array coordination procedure of Section 4.3 based on mapping skill requires extensive evaluation of the skill of different potential sampling arrays. We show here a procedure to dramatically reduce the computations required to invert large data–data covariances needed to evaluate the skill gradient as required.

We begin with the evaluation of skill after the previous step (the Nth) using (15), which requires the inverse of the order-N covariance with elements $\langle d_n d_m \rangle$. Also needed is the skill after

the next datum d_{N+1} is added. The minimum-square-error linear estimate of this datum (repeated lower-case indices indicate summing) is

$$\hat{d}_{N+1} = d_n D_{nm}^{-1} \langle d_m d_{N+1} \rangle. \tag{A.1}$$

Subtracting the part of d_{N+1} determined by N data gives the "innovation" of this datum:

$$d' = d_{N+1} - d_n D_{nm}^{-1} \langle d_m d_{N+1} \rangle. \tag{A.2}$$

This is uncorrelated with all other data so that the least-expected-square-error estimate of w from $N+1$ data is the estimate based on N data plus the estimate based on d':

$$\hat{w} = d_n D_{nm}^{-1} \langle d_m w \rangle + d' \langle d' w \rangle / \langle d'^2 \rangle. \tag{A.3}$$

The skill from $N+1$ data is

$$Q = \langle w d_n \rangle D_{nm}^{-1} \langle d_m w \rangle + \langle w d' \rangle^2 / \langle d'^2 \rangle, \tag{A.4}$$

where the first term on the rhs is recognized from (15) as the skill from the first N data and the second term is the skill added by datum $N+1$. This added skill Q' is

$$Q' = \frac{\langle w d' \rangle^2}{\langle d'^2 \rangle} = \frac{(\langle w d_{N+1} \rangle - \langle w d_n \rangle D_{nm}^{-1} \langle d_m d_{N+1} \rangle)^2}{(\langle d_{N+1}^2 \rangle - \langle d_{N+1} d_n \rangle D_{nm}^{-1} \langle d_m d_{N+1} \rangle)}. \tag{A.5}$$

Evaluating $\nabla \hat{\Sigma}$ involves the skill from a minimum of three additional potential points for d_{N+1} after D_{nm}^{-1} has been found for N data. This is much more rapidly evaluated from (A.5) than by inverting the order $N+1$ covariance, particularly if the repeated appearance of the vector $D_{nm}^{-1} \langle d_m d_{N+1} \rangle$ in (A.5) is noted.

References

Bergot, T., Doerenbecher, A., 2002. A study of the optimization of targeted observations using adjoint-based methods. Quarterly Journal of the Royal Meteorological Society 128, 1689–1712.

Bishop, C.H., Etherton, B.J., Majumdar, S.J., 2001. Adaptive sampling with the ensemble transform Kalman filter. Pt. I: theoretical aspects. Monthly Weather Review 129, 420–436.

Bretherton, F.P., Davis, R.E., Fandry, C.B., 1975. A technique for objective analysis and design of oceanographic experiments. Deep-Sea Research 23, 559–582.

Buizza, R., Montani, A., 1999. Targeted observations using singular vectors. Journal of the Atmospheric Sciences 56, 2965–2985.

Curtin, T.B., Bellingham, J.G., 2008. Progress toward autonomous ocean sampling networks. Deep-Sea Research II, this issue [doi:10.1016/j.dsr2.2008.09.005].

Davis, R.E., Eriksen, C.C., Jones, C.P., 2002. Autonomous buoyancy-driven underwater gliders. In: Griffiths, G. (Ed.), The Technology and Applications of Autonomous Underwater Vehicles. Taylor & Francis, London, p. 324pp.

Fiorelli, E., Leonard, N.E., Bhatta, P., Paley, D., Bachmayer, R., Fratantoni, D.M., 2006. Multi-AUV control and adaptive sampling in Monterey Bay. IEEE Journal of Oceanic Engineering. 31 (4), 935–948.

Leonard, N.E., Paley, D., Lekien, F., Sepulchre, R., Fratantoni, D.M., Davis, R., 2007. Collective motion, sensor networks, and ocean sampling. Proceedings of the IEEE 95 (1), 48–74.

Lermusiaux, P.F.J., 2007. Adaptive modeling, adaptive data assimilation and adaptive sampling. Physica D 230, 172–196.

Majumdar, S.J., Bishop, C.H., Etherton, B.J., 2002. Adaptive sampling with the ensemble transform Kalman filter. Pt. II: field program implementation. Monthly Weather Review 130, 1356–1369.

Pierce, A.D., 1989. Acoustics, An Introduction to its Physical Principles and Applications. Acoustical Society of America, Woodbury, NY.

Ramp, S.R., Davis, R.E., Leonard, N.E., Shulman, I., Chao, Y., Robinson, A.R., Marsden, J., Lermusiaux, P., Fratantoni, D., Paduan, J.D., Chavez, F., Bahr, F.L., Liang, S., Leslie, W., Li, Z., 2008. Preparing to predict: the second autonomous ocean sampling network (AOSN-II) experiment in the Monterey Bay. Deep-Sea Research II, this issue [doi:10.1016/j.dsr2.2008.08.013].

Stommel, H., 1989. The Slocum Mission. Oceanography April, 22–25.